Endosomal activation of the *Clostridioides difficile* binary toxin is Ca^{2+}-dependent.

Dinendra L. Abeyawardhane[1,2,3], Kaylin A. Adipietro[1,2,3], Raquel Godoy-Ruiz[1,2,3], Kristen M. Varney[1,2,3], Spiridon E. Sevdalis[1,3], Izza F. Nawaz[1], Alejandro X. Spittel[1], Richard R. Rustandi[4], Vitalii I. Silin[2,5], Amedee des Georges[6,7,8], Edwin Pozharski[1,2,3]*, and David J. Weber[1,2,3]*

[1]Department of Biochemistry and Molecular Biology, University of Maryland School of Medicine; Baltimore, MD 21201. [2]University of Maryland - Institute for Bioscience and Biotechnology Research; Rockville, MD 20850. [3]The Center for Biomolecular Therapeutics, The University of Maryland School of Medicine; Baltimore, MD 21201. [4]Merck & Co., Inc.; Kenilworth, NJ 07033. [5]National Institute of Standards and Technology; Gaithersburg, MD 20899. [6]Structural Biology Initiative, CUNY Advanced Science Research Center; New York, NY 10031. [7]Department of Chemistry and Biochemistry, City College of New York; NY 10031. and [8]PhD Programs in Biochemistry, and Chemistry, Graduate Center, City University of New York; NY 10016.

*To whom correspondence should be addressed.

Email: epozharskiy@som.umaryland.edu or dweber@som.umaryland.edu

One-sentence summary. Ca^{2+} dissociation and dynamics in a receptor binding domain activates pore-formation by *C. difficile* binary toxin.

Abstract. Pore formation via the CDTb cell-binding component of the *C. difficile* binary toxin (CDT) was discovered to be activated by depleting free Ca^{2+} ion concentrations, and not by lowering pH, as found for other binary toxins (i.e., anthrax). Cryoelectron microscopy, nuclear magnetic resonance spectroscopy, surface plasmon resonance, electrochemical impedance spectroscopy, CDT toxicity studies, and site directed mutagenesis show that dissociation of Ca^{2+} from a site in receptor binding domain 1 (RBD1) of CDTb is sufficient to generate pores in lipid bilayers. These data are consistent with a molecular mechanism in which Ca^{2+} dissociation from RBD1 provides a "conformational trigger" for CDTb to form pores as Ca^{2+} concentrations lower during endosomal delivery of CDT.

The Centers for Disease Control and Prevention identified *Clostridioides difficile* infection as one of the five most urgent bacterial threats to address in the United States. *Clostridioides difficile* is a gram-positive anaerobic bacterial pathogen responsible for a high-risk nosocomial disease prevalent among patients undergoing prolonged antibiotic treatments and/or cancer therapy (*1*). Reduced levels of symbiotic gut microbiota cause dominance of *C. difficile* bacteria that can lead to severe diarrhea and pseudomembranous colitis (*2*). Eradication of this bacterial pathogen is difficult due to highly stable spores and because therapeutic options are available only for the large clostridial toxins, TcdA (Toxin A) and TcdB (Toxin B) in CDI (*3, 4*). Problematic is that CDIs associated with hypervirulence and high recurrence rates often have a third toxin termed the *C. difficile* transferase (CDT) for which no treatment options are available (*5*). Studies *in vivo* of CDT-containing toxins show unambiguously that targeting the binary toxin, in addition to the large clostridial toxins, is required for achieving protection from hypervirulent CDI strains having all three toxins *(6).*

CDT enters host cells via endosomal delivery as do many other 'AB'-type binary toxins including *Clostridium perfringens*, *Clostridium spiroforme*, *Clostridium botulinum*, and *Bacillus anthracis* (*7-9*). The CDTb component of CDT binds to host cell surface and to host cell receptors to translocate the toxic enzymatic component of the binary toxin, termed CDTa, into the cytosol from endosomes. Upon cellular entry, the CDTa ribosyltransferase modifies host cell actin resulting in its depolymerization, destruction of cytoskeleton, and host cell death. CDTa (47.4 kDa) is composed of an N-terminal domain that binds to CDTb and a C-terminal catalytic domain (*10*). Full length pro-CDTb (99 kDa) undergoes proteolytic cleavage by trypsin/chymotrypsin to form active CDTb subunits (75 kDa). Under soluble conditions and at millimolar Ca^{2+} ion concentrations, as found in the extracellular environment, CDTb subunits can oligomerize into two highly stable "dumbbell-shaped" dimer of heptamers, into what is hypothesized as being a "protective" feature against CDTb subunit degradation prior to host cell binding (*11*). The two di-heptameric structures are distinct and include an asymmetric and a symmetric form (*11*). In asymmetric CDTb, one heptamer unit contains an extended β-barrel assembly originating from the heptameric core. Symmetric CDTb unit lacks the β-barrel extension and displays a uniform assembly of two identical heptamer units. The di-heptamer assembly involves a "donut-shaped" tetradecamer of what is termed receptor binding domain 2 (RBD2). Symmetric CDTb displays an "open" state while the asymmetric CDTb structure shows a "closed" pore-forming state with an extended β-barrel from one heptamer unit protected by receptor binding domains from the other associated heptamer (*12*). The terms open/closed reflect the inner diameter of the so-called φ-gate formed by seven phenylalanine side chains at the very center of the channel traversing the protein core, along which the enzyme payload is proposed to be translocated into cytosol from endosomes in an unfolded form.

While several structures of CDTa, CDTb, and the CDTa/CDTb complex are available (*10, 13, 14*), the molecular mechanism for CDT delivery into host cells remains uncertain. Based on the mode of action established for anthrax toxin, it was anticipated that CDTb

would undergo a conformational shift facilitated by acidic pH in the early endosomal compartments to facilitate transport of the catalytic component, CDTa, into the cytosol (*15*). However, we show that lowering pH is alone not sufficient for CDTb to bind membrane and form pores, as found for the analogous cell-binding subunit of the anthrax toxin termed the protective antigen (PA). Whereas the studies reported here examine CDTb membrane-binding and pore formation and identified a role in this process for Ca^{2+}-binding to a site discovered in its receptor binding domain 1 (RBD1) that is also important for regulating RBD1 folding.

Membrane binding and pore formation by CDTb, the cell-binding component CDT. A fundamental question is whether the CDTb cell-binding component of CDT can insert into membrane bilayers and form pores on its own, as found for other members of the A-B toxin family, such as the protective antigen (PA) of anthrax (*16, 17*). This question was addressed using a combination of surface plasmon resonance and electrochemical impedance spectroscopy (SPR/EIS). A custom-built experimental platform was used to measure CDTb adsorption/desorption at the biomimetic tethered bilayer lipid membrane via a change of SPR signal while measurement of electrical resistance of the bilayer via EIS was recorded in parallel (*18, 19*). Like for anthrax, it was anticipated that CDTb may undergo a conformational change facilitated by acidic pH upon entry into early endosomal compartments to facilitate transport of the catalytic component, CDTa, into the cytosol (*15*). Cellular uptake of *C. perfringens* iota toxin and *C. botulinum* C2 toxin are also facilitated by acidification (*20, 21*). Therefore, we lowered the pH to match values typically found in endosomes (~pH 5.5) and examined whether CDTb insertion into membrane and pore formation could be observed using EIS upon binding to POPC-based-tethered bilayer lipid membrane, which is the major constituent of endosomal membrane (*22*). However, unlike what was found for the anthrax toxin (*23, 24*), CDTb did not bind lipid bilayers or form pores in the membrane-like vesicles upon lowering pH to acidic values as was found for anthrax protective antigen, which was measured here as a positive control (Fig. S12).

In addition to pH lowering upon endosomal compartmentalization, Ca^{2+} ion concentrations decrease from values in the millimolar range, as found in extracellular space, to low micromolar levels as measured in endosomes (*25*). We therefore examined whether lowering free Ca^{2+} concentration enabled CDTb binding to lipid bilayers and CDTb-dependent pore formation. This hypothesis was intriguing considering a newly discovered Ca^{2+}-binding site in the CDTb (Fig. S1) enables the RBD1 domain to undergo conformational exchange between a folded and dynamic state as Ca^{2+} ion concentrations decrease to those found in endosomes (*11*). To test this hypothesis, we dialyzed the CDTb protein against a buffer containing 2 mM of EDTA and EGTA to decrease free Ca^{2+} ion concentration and increase the conformational dynamics within RBD1. As demonstrated by simultaneous increases in SPR signal and electrical conductance by EIS (Fig. 1B), Ca^{2+} depleted CDTb ($CDTb^{(-Ca)}$) was found to adsorb into the phospholipid membrane and form a pore that generates an influx of ions at pH 5.5. The membrane binding data together with the increase in EIS signal signifies evidence for channel

formation upon CDTb addition at depleted Ca^{2+} ion concentrations and supports the hypothesis that Ca^{2+} ion depletion triggers membrane insertion of the CDTb translocase. Whereas the analogous experiments done in the presence of millimolar Ca^{2+} ion concentrations showed negligible changes in SPR signal and electrical conductance, indicating that neither membrane binding nor pore-formation occurs at elevated Ca^{2+} concentrations with fully stabilized CDTb (Fig. 1A).

CryoEM structures of CDTb in a Ca^{2+}-depleted state. Structural studies showed previously that there are at least three Ca^{2+}-binding sites on CDTb at mM Ca^{2+} levels as found in the extracellular environment (*11*). This includes two high-affinity Ca^{2+} ion sites in the N-terminal heptamerization domain of CDTb (HD1), which are conserved in anthrax toxin PA and iota toxin Ib, and are essential for binding of the enzymatic component of the binary toxin (*26, 27*). The third Ca^{2+}-binding site in CDTb is weaker and involves coordinating residues from within RBD1 of CDTb (Fig. S1). The RBD1 Ca^{2+} binding site was of interest here, as it was critical for conformational exchange within the RBD1 domain as Ca^{2+} concentrations were decreased (*11*). Thus, it was hypothesized that Ca^{2+} unbinding from this same RBD1 site, which coincides with an increase in its conformational dynamics, could "trigger" CDTb membrane binding and pore formation.

To test this "Ca^{2+} unbinding" hypothesis further, we solved the structure of wild-type CDTb sample that was dialyzed versus buffer containing 2 mM of EDTA/EGTA using single-particle cryo-electron microscopy (Fig. 2). While these conditions were sufficient to remove Ca^{2+} from the weaker RBD1 site, the higher-affinity dual Ca^{2+} ion binding sites in the HD1 domain of CDTb remained intact (Fig. S3). That Ca^{2+} binding to HD1 was not disrupted by this sample preparation was consistent with reports that disrupting Ca^{2+}-binding to HD1 required harsh denaturing conditions for their removal (*28*). Thus, the milder dialysis conditions used here to remove Ca^{2+} from RBD1 did not affect Ca^{2+} binding to HD1 nor did such conditions disrupt the structural integrity of the heptamerization core of CDTb (Fig. 2).

Initial 2D classification for Ca^{2+}-depleted CDTb revealed the presence of a single heptamer unit, and subsequent 3D refinement found two distinct structural moieties derived from the "pore-forming" conformation of CDTb (Fig. 2). The difference between the two structures was the degree of flexibility observed for RBD2. An RBD2 distorted structure (class 1) was solved at a resolution of 3.06 Å and the heptamer structure with RBD2 intact (class 2) was solved at 3.28 Å resolution (Fig. 2 and Fig. S2). While the elongated β-barrel was not observed in either structure, partial β-barrel formation was detected. As expected, the RBD1 domains in both structures were mobile as is consistent with Ca^{2+} removal from the RBD1 site when this domain was isolated (9). It is interesting that the two Ca^{2+}-depleted structures solved (classes 1, 2) both closely resemble the "pre-insertion" states recognized previously for CDTb (*14*).

Structure/function studies of a Ca^{2+}-binding mutant of CDTb. We next examined CDTb constructs that eliminated Ca^{2+}-binding to RBD1 via a D623A/D734A double mutation (Fig. S1). We first showed by 2D ^{1}H-^{15}N heteronuclear single quantum

coherence (HSQC) NMR that the D623A/D734A double mutation was sufficient to eliminate Ca^{2+} binding to ^{15}N-labeled RBD1$^{D623A/D734A}$, as engineered ($^{Ca}K_D$ >10 mM), at both pH 5.0 and 7.0 (Figs. S4 and S5). Importantly, in the absence of Ca^{2+}, the 2D ^{1}H-^{15}N HSQC data for RBD1$^{D623A/D734A}$ exhibited significant exchange broadening at both acidic and neutral pH values (pH 5.0 and 7.0). Whereas upon 10 mM Ca^{2+} addition, no significant changes in the HSQC spectra were observed for RBD1$^{D623A/D734A}$ at either pH value, as compared to wild-type protein (Fig. 3). Specifically, upon 10 mM Ca^{2+} addition to the wild-type construct (^{15}N-labeled RBD1^{WT}), highly dispersed HSQC spectra appeared at both pH 5.0 and pH 7.0 (Fig. 3 and Fig. S6) as found previously for RBD1^{WT} at pH 7.4 (*11*). The Ca^{2+}-binding studies by NMR were confirmed via monitoring changes in tryptophan fluorescence whereby Ca^{2+}-binding to RBD1^{WT} was observed ($^{Ca}K_D$ = 120 $\pm$ 20 μM; Fig. 4). Whereas no detectable effect on tryptophan fluorescence was observed for RBD1$^{D623A/D734A}$ upon Ca^{2+} ion addition even at concentrations as high as 10 mM ($^{Ca}K_D$ > 10 mM). Under identical conditions, toxicity to *Vero* cells was compared next upon addition of binary CDT having either full-length CDTb^{WT} or CDTb$^{D623A/D734A}$, respectively. The optimal CDTa to CDTb ratio for CDT was maintained at a 1:7 ratio, respectively, throughout the assay for both toxin constructs as described previously (*29*). In these studies, only an ~8-fold decrease in cytotoxicity was detected for CDTb$^{D623A/D734A}$ (TC_{50} = 560±60 pM) versus CDTb^{WT} (TC_{50} = 70±20 pM) (Fig. S7). Importantly, cytotoxicity studies showed that CDT retained a highly potent cytotoxic effect even when the Ca^{2+}-binding site of RBD1 was mutated (Fig. 5), which is consistent with a Ca^{2+}-free RBD1 domain being sufficient for delivering a highly toxic effect in the pM range.

Notably the structure of CDTb$^{D623A/D734A}$ was solved and found to be a single heptamer at 3.56 Å resolution (Fig. 5), much like that found for the CDTb structure solved under Ca^{2+}-depleted states. Of notable interest is that the structure of CDTb$^{D623A/D734A}$ lacks clear density for the RBD1 and RBD2 domains consistent with these domains being dynamic when the RBD1 Ca^{2+} ion binding site is mutated. Interestingly, the observed heptameric structure of CDTb$^{D623A/D734A}$ resembles a single 'pore-forming state' with an elongated β-barrel assembly (Fig. S8). Of further interest, our structures illustrate the existence of a single heptamer unit in soluble conditions for the first time, without detergents or lipid membrane-like support (Fig. 5*C*). That isolated RBD2 is monomeric in solution and crystallizes as a monomer further demonstrates that the donut-shaped RBD2 structure found in the di-heptamer oligomerization states is assisted by the heptamerization and that RBD1 domains stabilize the overall protein framework (*11*). Together these data are consistent with a mechanism by which increased flexibility of RBD1 upon Ca^{2+} removal results in destabilization of the RBD2 domain position, thus disrupting CDTb di-heptamer formation and further facilitating CDTb membrane binding and pore formation on its own. Such a mechanism of action could facilitate receptor interactions via membrane-lateral diffusion in a 2- versus 3-dimensional approach, as is the case for other beta-barrel forming bacterial toxins (*30*).

Interestingly, the β-barrel domain of CDTb (residues 298 to 401) originates from the heptameric core and elongates to form a "stem-like" structure that is essential for

membrane insertion. The CDTb$^{D623A/D734A}$ structure depicted weaker density at the end of the β-barrel and therefore residues ranging from 332 to 362 could not be modeled (Fig. 5*B*). This could be due to partial unfolding of the tip of the β-barrel in the absence of supporting membrane structure and/or from some of the dynamic features associated with the lack of Ca^{2+} bound to RBD1. Also intact was the structural orientation of Phe455, the key residue in "φ-gate" assembly, which in this structure agrees with the narrowest 6 Å clamp identified for the CDTb pore state (Fig. S9).

Coincidentally, the receptor binding domains (RBD1 and RBD2) were relatively disordered in CDTb$^{D623A/D734A}$, as compared to wild-type CDTb (9) and modeling partial density in RBD1 for the double mutant could not be achieved globally. Although, when the CDTb$^{D623A/D734A}$ map was examined with C1 symmetry, the occurrence of stronger RBD1 density was noticed in one or two of the protomers versus others (Fig. S10); whereas application of C7 symmetry averaged out density in all the RBD1 protomers among the seven subunits. Thus, the absence of a bound Ca^{2+} ion in the RBD1 domain of CDTb$^{D623A/D734A}$ leads to a less defined structure in the RBD domains than for wild-type CDTb, and the increased flexibility of RBD1 in the CDTb$^{D623A/D734A}$ Ca^{2+} binding site mutant was found to affect stability of the RBD2 domains and prevent observation of the assembly of RBD2 "donut" structures observed previously for the wild type di-heptamer CDTb structures (9).

Ca^{2+} depletion upon CDTb entering early endosomes can trigger CDTb membrane binding and pore formation. From the CDTb structures presented here, we highlight that removal of the Ca^{2+} site in RBD1 by mutation or Ca^{2+} dissociation via dialysis results in a functional CDTb binary toxin component at pM levels. To understand better why low pH alone does not trigger pore formation, as observed for anthrax toxin, we compared the superimposed prepore and pore states of CDTb and anthrax PA. While heptamerization core is well aligned in both proteins, a key difference in the β-barrel forming domain was detected in the prepore state overlay (Fig. S11). A direct link of β-barrel domain and RBD1 in CDTb restricts mobility of the β-loop and stabilizes the prepore assembly. Therefore, Ca^{2+} removal sacrifices the stability of RBD1, triggering a conformational rearrangement in the CDTb membrane insertion β-loop to transition from prepore state to pore state. Thus, the overall mechanism for RBD1 Ca^{2+}-sensing is that RBD1's stable Ca^{2+} bound conformation forms direct interactions with the β-barrel domain, locking it into an orientation that is folded into the heptamerization domain. Whereas Ca^{2+} depletion in maturing endosomes unfolds RBD1, thus freeing the β-barrel domain to reassemble into the heptameric pore conformation (Fig. 6).

In summary, the data presented here are consistent with a novel mechanism of host cell engagement by the cell-binding and toxin delivery component of the binary toxin, CDTb. Specifically, Ca^{2+}-dissociation from the RBD1 domain of CDTb or mutation of this site were found to be sufficient for this component of CDT to bind and pierce membrane bilayers. Such a mechanism of action can be understood at atomic detail as it is clear by NMR and cryoEM studies that dissociation of Ca^{2+} from this RBD1 site induces

conformational dynamics that directly impact a di-heptamer to heptamer transition and/or membrane binding. Physiologically, these findings are consistent with a molecular mechanism in which entry of CDTb into early endosomes is sufficient for Ca^{2+}-dissociation from RBD1 followed by CDTb binding and pore formation. Also shown is that the absence of Ca^{2+} bound to the RBD1 site provides a heptamer that is highly dynamic, which may be important for these molecular events. Thus, the results presented here show that CDTb membrane binding and pore formation can occur upon Ca^{2+} dissociation from RBD1 of CDTb and represents a novel and important first step towards clarifying how the presence of host cell receptors and/or CDTa binding impacts CDT delivery into its cellular host. This work also suggests that diverse mechanisms are used by bacterial translocases of this class to trigger timely activation in maturing endosomes. Finally, whether acidic pH (pH < 6) affects CDT entry and/or receptor mediated CDT entry into host cells in addition to Ca^{2+} dissociation from CDTb requires further study.

ACKNOWLEDGMENTS. Funding by NIH (R56 AI152397; DJW and AdG; R01 GM129327 to DJW), from the Center for Biomolecular Therapeutics (D.J.W.), the Maryland Center for Advanced Molecular Analyses (D.J.W. and E.P.), University of Maryland - Institute for Bioscience and Biotechnology Research (IBBR), and the University of Maryland School of Medicine are acknowledged. This research is also supported in part by funds through the Maryland Department of Health's Restitution Fund Program (CH-649-CRF), and NCI-CCSG (P30CA134274). The National Institute of Standards and Technology (NIST) Center for Nanoscale Science and Technology cleanroom in Gaithersburg, MD is acknowledged for the preparation of chips needed for SPR/EIS experiments. Finally, we express our appreciation to John J. Kasianowicz for sharing the SPR/EIS data collected for anthrax toxin.

Author Contributions:

Conceptualization: EP, AdG, DJW

Methodology: DLA, KAA, RG-R, KMV, SES, IFN, AXS, RRR, VIS, EP, and DJW

Investigation: DLA, KAA, RG-R, KMV, SES, IFN, AXS, RRR, VIS, AdG, EP, and DJW

Funding acquisition: EP, AdG, DJW

Supervision: EP, KMV, VIS, DJW

Writing – original draft: DLA, KAA, RG-R, KMV, SES, RRR, VIS, EP, and DJW

Writing – review & editing: DLA, KAA, RG-R, KMV, SES, RRR, VIS, AdG, EP, and DJW

Competing Interest Statement: The authors declare no competing interest.

Data deposition: Cryoelectron microscopy density maps have been deposited in the Electron Microscopy Data Bank (EMDB), https://www.ebi.ac.uk/pdbe/emdb/ (accession nos. EMD- 28207 for $CDTb^{D623A/D734A}$, EMD- 28206 for $CDTb^{(-Ca)}$ class 1 and EMD- 28205 for $CDTb^{(-Ca)}$ class 2). Model coordinates have been deposited in the Protein Data Bank (PDB), https://www.wwpdb.org/ (PDB ID codes 8EKM for $CDTb^{D623A/D734A}$, 8EKL for $CDTb^{(-Ca)}$ class 1, and 8EKK for $CDTb^{(-Ca)}$ class 2). All other data are available from the corresponding authors upon request.

Figures.

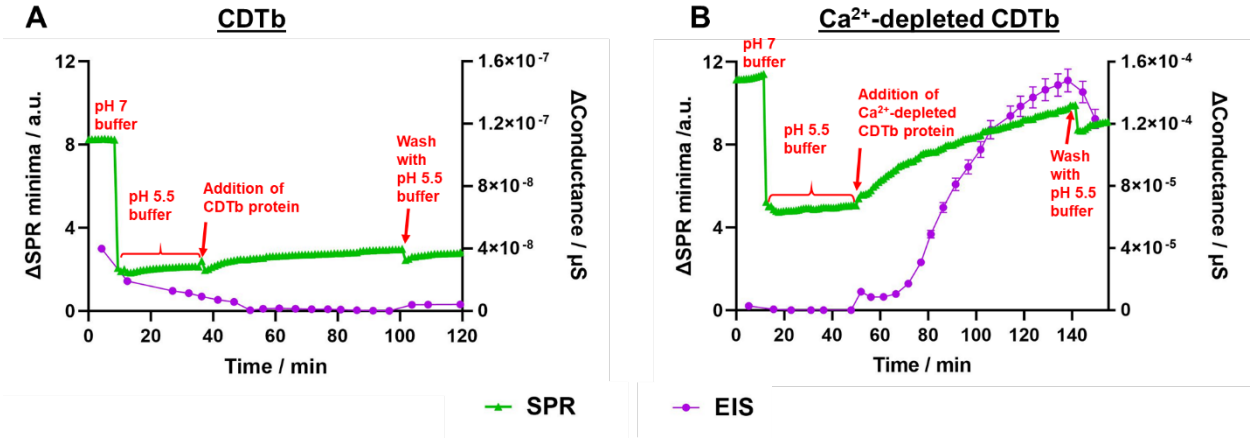

Fig. 1. Membrane interactions of CDTb variants at pH 5.5 studied by surface plasmon resonance (SPR, green triangles) coupled to electrochemical impedance spectroscopy (EIS, purple spheres) collected in the (A) absence or (B) presence of the calcium ion chelator EGTA (see Methods).

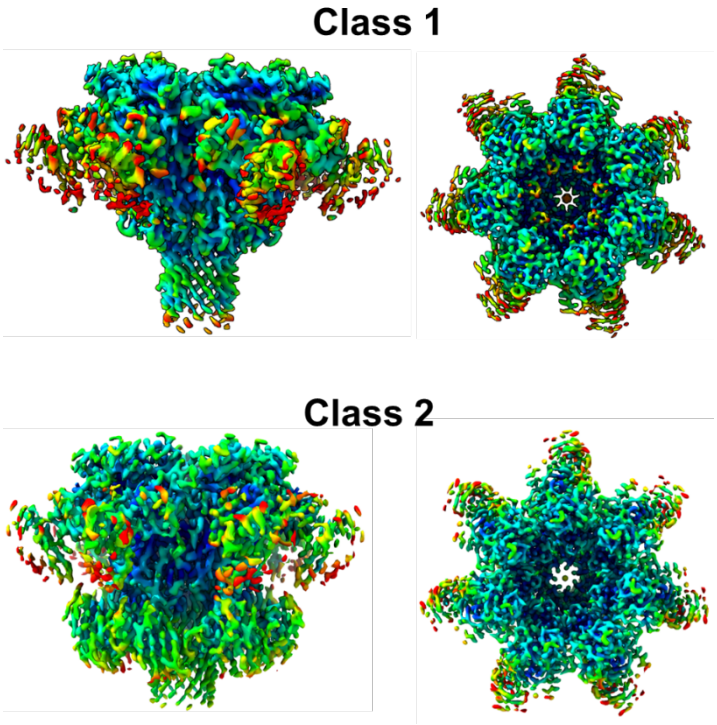

Fig. 2. Local resolution in electron density maps of CDTb$^{(-Ca)}$ conformations; RBD2 distorted structure (class 1) and the heptamer with RBD2 intact (class 2). The difference in the degree of RBD2 is distinguishable by side and top projections of each class.

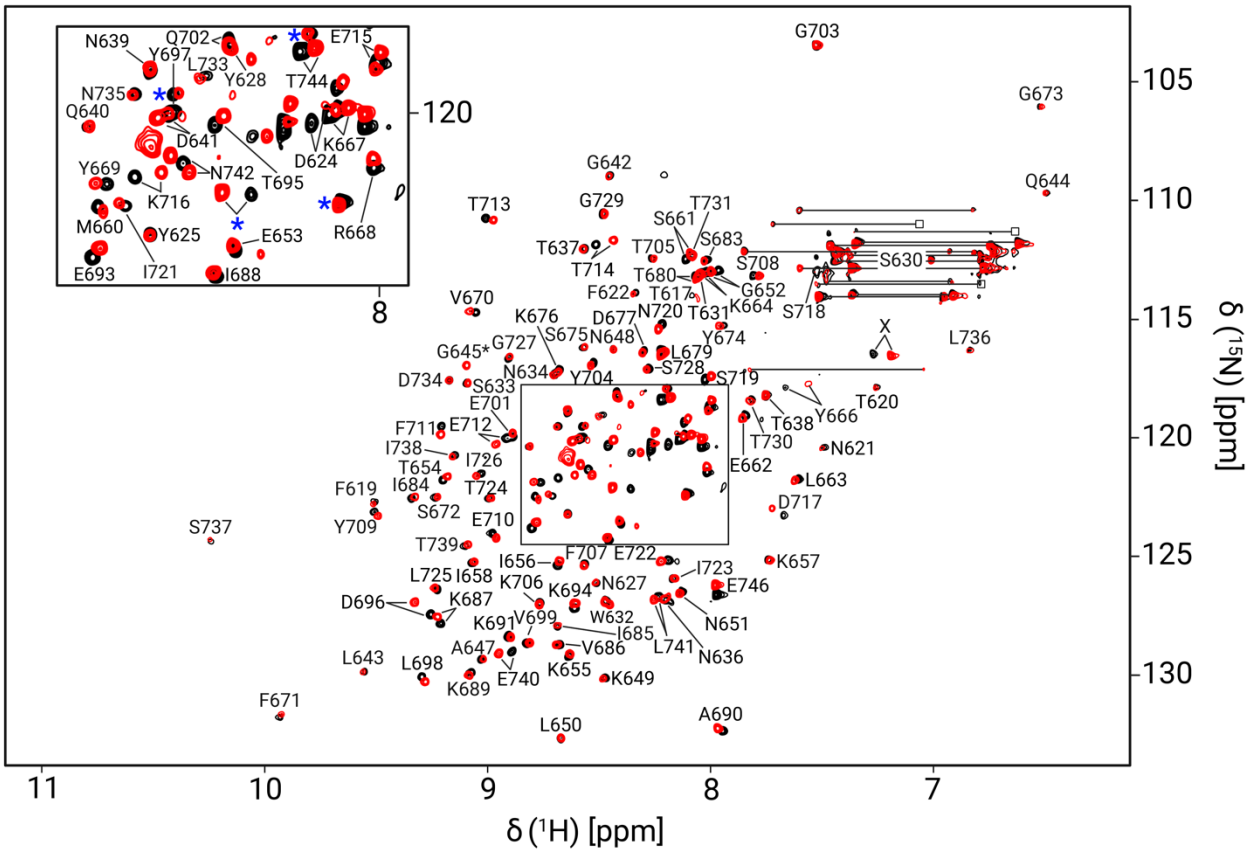

Fig. 3. Overlay of ^{15}N-HSQC NMR spectra of RBD1^{WT} (0.1 mM) at pH 7.0 (black) and pH 5.0 (red) after 20 hours incubation with 10 mM Ca^{2+}. Residues marked by blue asterisks are associated with the His-tag. The assignment for the contour marked "X" could not be confirmed fully as correlations to this H^N were very weak in several of the 3D NMR data sets. The contour labeled as G645, and with a black asterisk (*) appeared in the noise at pH 7.0 but became stronger as the pH decreased. Correlations connected by horizontal lines correspond to sidechain NH_2 groups.

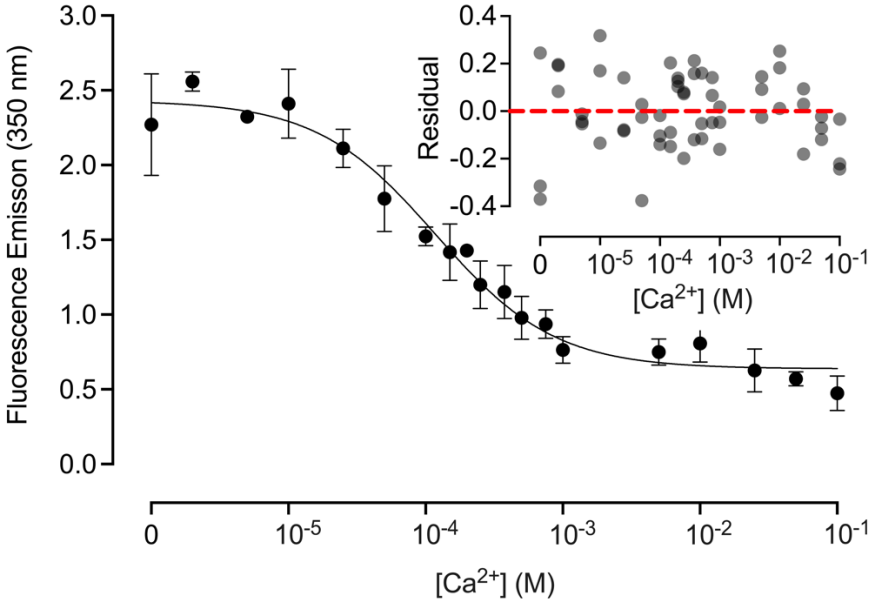

Fig. 4. Calcium ion binding to wild-type RBD1. Ca^{2+}-binding to the RBD1 domain (residues 616 - 748) was monitored by changes in fluorescence intensity of the single tryptophan residue in RBD1 (i.e., W632; ${}^{Ca}K_D = 120 \pm 20\ \mu M$). A residual plot for the data fitting to a model with noncooperative binding to a single site in RBD1 is shown in the upper right corner.

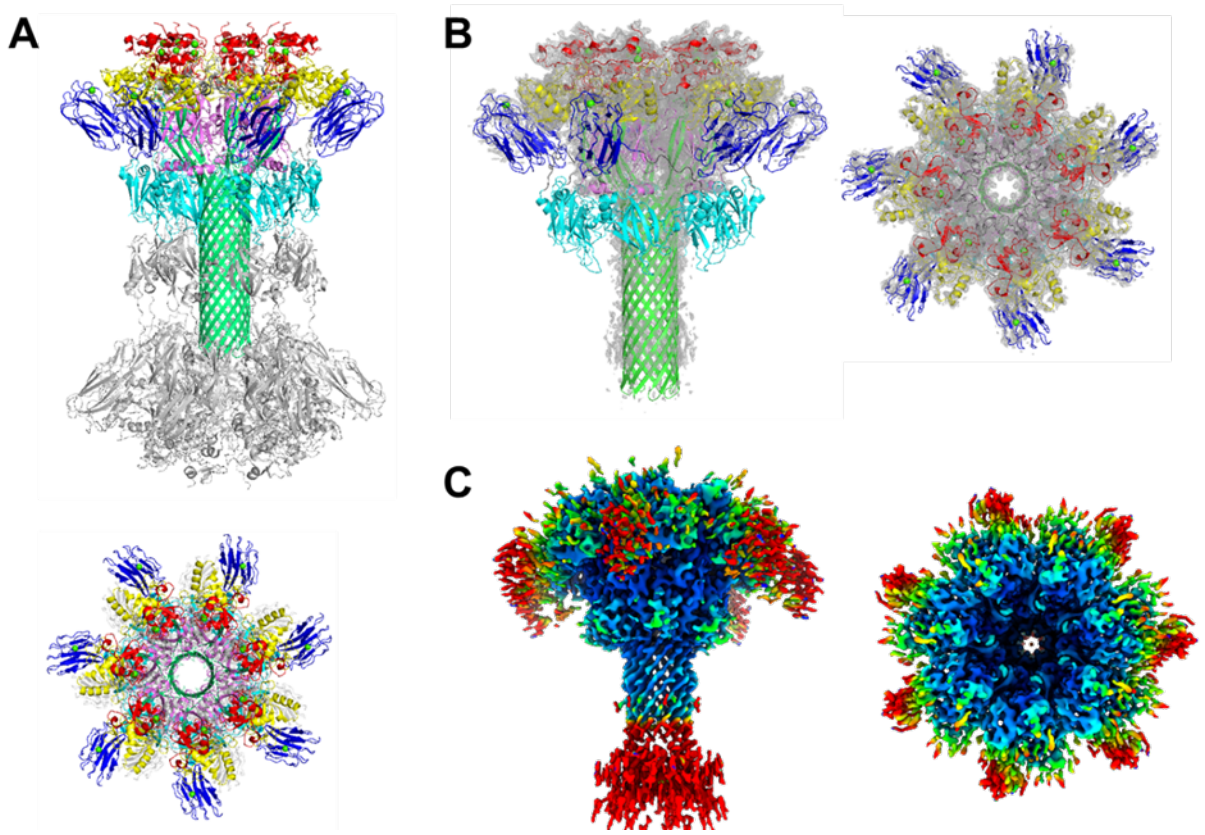

Fig. 5. Comparison of the structural architecture of the CDTb and the CDTb$^{D623A/D734A}$. (*A*) Side and top projections of the di-heptamer structure in the "asymmetric form" of CDTb (PDB: 6UWR). The heptamer with the β-barrel extension is illustrated in different colors; heptamerization domain 1 (HD1; residues 212-297) in red, β-barrel domain (βBD; residues 298-401) in green, heptamerization domain 2 (HD2; residues 402-486) in violet, linker region 1 (L1; residues 487-513) in grey, heptamerization domain 3 (HD3; residues 514-615) in yellow, receptor binding domain 1 (RBD1; residues 616-744) in blue, linker region 2 (L2; residues 745-756) in grey, and receptor binding domain 2 (RBD2; residues 757-876) in cyan. Dual Ca^{2+} ions are bound in HD1 and the single Ca^{2+} ion bound in RBD1 are shown as green spheres. (*B*) The single heptamer extracted from CDTb is superimposed with the electron mesh map of the CDTb$^{D623A/D734A}$ structure. (*C*) The electron density map of CDTb$^{D623A/D734A}$ is colored by local resolution with C7 symmetry imposed. Increased flexibility is observed in the outer regions of the core heptamer, and it is most pronounced for the RBD1 domain and the tip of the β-barrel extension.

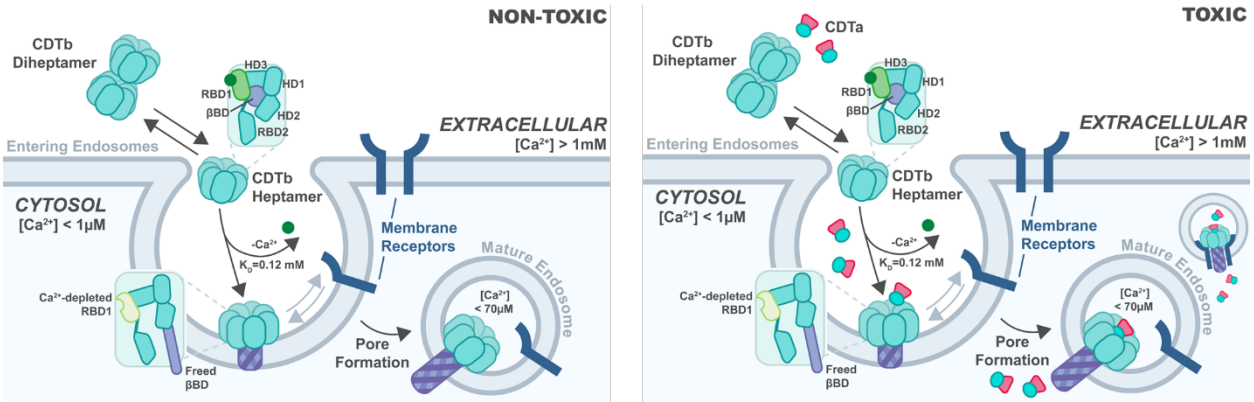

Fig. 6. Models for membrane association and pore-formation for CDTb alone (non-toxic) and in the presence of CDTa (toxic). These schematics show the importance of having a therapeutic strategy that disrupts CDT prior to entering mature endosomes. (A; left) In an extracellular environment ([Ca^{2+}] > 2 mM), CDTb exists in an equilibrium between single CDTb subunits and two diheptamer structures with no observable heptamer oligomers (*11*). Upon dissociation of Ca^{2+} from the RBD1 domain of CDTb ($^{Ca}K_D$ = 120 ± 20 μM), the RBD1 domain enters conformational exchange allowing the β-barrel forming residues to reassemble as needed to bind membrane and form pores in the lipid bilayer. A change in orientation of beta-barrel forming residues (purple) within single subunits of the CDTb heptamer are presented as CDTb transitions from an extracellular (pH = 7.4 and [Ca^{2+}] > 1 mM) to an endosomal environment (pH ~ 5.5 and [Ca^{2+}] < 1 μM). The membrane-penetrating partial β-barrel (pre-insertion state) formation is initiated upon endocytosis. Low internal Ca^{2+} concentration (< 70 μM) and acidic pH (~ 5.5) in the endosome ensure the membrane-spanning pore formation with the complete extended β-barrel. The *right* panel illustrates components needed for a "toxic" outcome with CDTa present under cellular conditions. The pathway for pore formation of CDTb occur in a similar manner to "non-toxic" model, but it is proposed that the CDTb-receptor interactions could be facilitated via membrane lateral diffusion of CDTb and/or receptor(s). However, a complete mechanism of action for CDTa delivery by CDTb within a mature endosome requires further examination of multiple equilibria and their corresponding structures where pH and [Ca^{2+}] values are unique as compared to intra- and extracellular environments.

References.

1. M. Rupnik, M. H. Wilcox, D. N. Gerding, Clostridium difficile infection: new developments in epidemiology and pathogenesis. *Nat Rev Microbiol* **7**, 526-536 (2009).
2. S. L. Kordus, A. K. Thomas, D. B. Lacy, Clostridioides difficile toxins: mechanisms of action and antitoxin therapeutics. *Nat Rev Microbiol*, (2021).
3. J. Czepiel *et al.*, Clostridium difficile infection: review. *Eur J Clin Microbiol Infect Dis* **38**, 1211-1221 (2019).
4. K. O'Grady, D. R. Knight, T. V. Riley, Antimicrobial resistance in Clostridioides difficile. *Eur J Clin Microbiol Infect Dis* **40**, 2459-2478 (2021).
5. S. Perelle, M. Gibert, P. Bourlioux, G. Corthier, M. R. Popoff, Production of a complete binary toxin (actin-specific ADP-ribosyltransferase) by Clostridium difficile CD196. *Infect Immun* **65**, 1402-1407 (1997).
6. S. Secore *et al.*, Development of a Novel Vaccine Containing Binary Toxin for the Prevention of Clostridium difficile Disease with Enhanced Efficacy against NAP1 Strains. *PLoS One* **12**, e0170640 (2017).
7. O. Knapp, R. Benz, M. R. Popoff, Pore-forming activity of clostridial binary toxins. *Biochim Biophys Acta* **1858**, 512-525 (2016).
8. K. Aktories, P. Papatheodorou, C. Schwan, Binary Clostridium difficile toxin (CDT) - A virulence factor disturbing the cytoskeleton. *Anaerobe*, (2018).
9. P. Papatheodorou, H. Barth, N. Minton, K. Aktories, Cellular Uptake and Mode-of-Action of Clostridium difficile Toxins. *Adv Exp Med Biol* **1050**, 77-96 (2018).
10. A. Sundriyal, A. K. Roberts, C. C. Shone, K. R. Acharya, Structural basis for substrate recognition in the enzymatic component of ADP-ribosyltransferase toxin CDTa from Clostridium difficile. *J Biol Chem* **284**, 28713-28719 (2009).
11. X. Xu *et al.*, Structure of the cell-binding component of the Clostridium difficile binary toxin reveals a di-heptamer macromolecular assembly. *Proc Natl Acad Sci U S A* **117**, 1049-1058 (2020).
12. D. L. Abeyawardhane *et al.*, The Importance of Therapeutically Targeting the Binary Toxin from Clostridioides difficile. *Int J Mol Sci* **22**, (2021).
13. M. J. Sheedlo, D. M. Anderson, A. K. Thomas, D. B. Lacy, Structural elucidation of the Clostridioides difficile transferase toxin reveals a single-site binding mode for the enzyme. *Proc Natl Acad Sci U S A* **117**, 6139-6144 (2020).
14. D. M. Anderson, M. J. Sheedlo, J. L. Jensen, D. B. Lacy, Structural insights into the transition of Clostridioides difficile binary toxin from prepore to pore. *Nat Microbiol* **5**, 102-107 (2020).
15. D. N. Gerding, S. Johnson, M. Rupnik, K. Aktories, Clostridium difficile binary toxin CDT: mechanism, epidemiology, and potential clinical importance. *Gut microbes* **5**, 15-27 (2014).
16. L. Abrami, M. Lindsay, R. G. Parton, S. H. Leppla, F. G. van der Goot, Membrane insertion of anthrax protective antigen and cytoplasmic delivery of lethal factor occur at different stages of the endocytic pathway. *J Cell Biol* **166**, 645-651 (2004).
17. J. Sun, G. Vernier, D. J. Wigelsworth, R. J. Collier, Insertion of anthrax protective antigen into liposomal membranes: effects of a receptor. *J Biol Chem* **282**, 1059-1065 (2007).
18. V. I. Silin, D. P. Hoogerheide, pH dependent electrical properties of the inner- and outer-leaflets of biomimetic cell membranes. *J Colloid Interface Sci* **594**, 279-289 (2021).
19. T. Vandenryt *et al.*, Combining electrochemical impedance spectroscopy and surface plasmon resonance into one simultaneous read-out system for the detection of surface interactions. *Sensors (Basel)* **13**, 14650-14661 (2013).
20. M. Gibert *et al.*, Differential requirement for the translocation of clostridial binary toxins: iota toxin requires a membrane potential gradient. *FEBS Lett* **581**, 1287-1296 (2007).

21. D. Blocker, C. Bachmeyer, R. Benz, K. Aktories, H. Barth, Channel formation by the binding component of Clostridium botulinum C2 toxin: glutamate 307 of C2II affects channel properties in vitro and pH-dependent C2I translocation in vivo. *Biochemistry* **42**, 5368-5377 (2003).
22. D. Casares, P. V. Escriba, C. A. Rossello, Membrane Lipid Composition: Effect on Membrane and Organelle Structure, Function and Compartmentalization and Therapeutic Avenues. *Int J Mol Sci* **20**, (2019).
23. V. Silin *et al.*, Biochip for the Detection of Bacillus anthracis Lethal Factor and Therapeutic Agents against Anthrax Toxins. *Membranes (Basel)* **6**, (2016).
24. A. Michelman-Ribeiro, K. A. Rubinson, V. Silin, J. J. Kasianowicz, Solution Structures of Bacillus anthracis Protective Antigen Proteins Using Small Angle Neutron Scattering and Protective Antigen 63 Ion Channel Formation Kinetics. *Toxins (Basel)* **13**, (2021).
25. T. Albrecht, Y. Zhao, T. H. Nguyen, R. E. Campbell, J. D. Johnson, Fluorescent biosensors illuminate calcium levels within defined beta-cell endosome subpopulations. *Cell Calcium* **57**, 263-274 (2015).
26. P. K. Gupta *et al.*, Conformational fluctuations in anthrax protective antigen: a possible role of calcium in the folding pathway of the protein. *FEBS Letters* **554**, 505-510 (2003).
27. K. Kobayashi *et al.*, Role of Ca2+-binding motif in cytotoxicity induced by Clostridium perfringens iota-toxin. *Microbial Pathogenesis* **44**, 265-270 (2008).
28. S. Gao-Sheridan, S. Zhang, R. J. Collier, Exchange characteristics of calcium ions bound to anthrax protective antigen. *Biochem Biophys Res Commun* **300**, 61-64 (2003).
29. J. Xie *et al.*, Development and optimization of a high-throughput assay to measure neutralizing antibodies against Clostridium difficile binary toxin. *Clin Vaccine Immunol* **21**, 689-697 (2014).
30. I. Ilangumaran Ponmalar, N. K. Sarangi, J. K. Basu, K. G. Ayappa, Pore Forming Protein Induced Biomembrane Reorganization and Dynamics: A Focused Review. *Front Mol Biosci* **8**, 737561 (2021).